2D divertor heat flux distribution using a 3D heat conduction solver in National Spherical Torus Experiment

K. F. Gan,[1] J-W. Ahn,[2,a)] J.-W. Park,[3] R. Maingi,[2] A. G. McLean,[4] T. K. Gray,[2] X. Gong,[1] and X. D. Zhang[1]
[1]*Institute of Plasma Physics, Chinese Academy of Sciences, Hefei, China*
[2]*Oak Ridge National Laboratory, Oak Ridge, Tennessee 37831, USA*
[3]*Department of Nuclear Engineering, Seoul National University, Seoul, Republic of Korea*
[4]*Lawrence Livermore National Laboratory, Livermore, California 94551, USA*

(Received 27 July 2012; accepted 4 February 2013; published online 21 February 2013)

The divertor heat flux footprint in tokamaks is often observed to be non-axisymmetric due to intrinsic error fields, applied 3D magnetic fields or during transients such as edge localized modes. Typically, only 1D radial heat flux profiles are analyzed; however, analysis of the full 2D divertor measurements provides opportunities to study the asymmetric nature of the deposited heat flux. To accomplish this an improved 3D Fourier analysis method has been successfully applied in a heat conduction solver (TACO) to determine the 2D heat flux distribution at the lower divertor surface in the National Spherical Torus Experiment (NSTX) tokamak. This advance enables study of helical heat deposition onto the divertor. In order to account for heat transmission through poorly adhered surface layers on the divertor plate, a heat transmission coefficient, defined as the surface layer thermal conductivity divided by the thickness of the layer, was introduced to the solution of heat conduction equation. This coefficient is denoted as α and a range of values were tested in the model to ensure a reliable heat flux calculation until a specific value of α led to the constant total deposited energy in the numerical solution after the end of discharge. A comparison between 1D heat flux profiles from TACO and from a 2D heat flux calculation code, THEODOR, shows good agreement. Advantages of 2D heat flux distribution over the conventional 1D heat flux profile are also discussed, and examples of 2D data analysis in the study of striated heat deposition pattern as well as the toroidal degree of asymmetry of peak heat flux and heat flux width are demonstrated. © *2013 American Institute of Physics*. [http://dx.doi.org/10.1063/1.4792595]

I. INTRODUCTION

The power handling capability of divertors is a crucial problem for tokamaks. Understanding of the characteristics of the heat flux divertor footprint is important for control of the peak heat flux deposition, which is of primary importance for the protection of divertor plates. The controlling physics for divertor heat flux are complicated since we still do not have a clear understanding of how the asymmetric power deposition occurs and its relation to intrinsic error fields, turbulence filaments, and the edge localized mode (ELM) which is a magnetohydrodynamic (MHD) instability occurring at the edge of plasma and causes non-axisymmetric divertor heat flux deposition. Infrared (IR) imaging diagnostics are useful tools for investigation of the 2D temperature distribution and power deposition onto the divertor surface. Heat flux analysis carried out in tokamaks to date has focused on 1D radial distribution, typically obtained from a finite difference code solving the heat conduction equation in 2D, i.e., in the direction of radius (r) and tile depth (z), such as THEODOR.[1–4] National Spherical Torus Experiment (NSTX) has applied THEODOR for 1D radial heat flux profiles over the past few years. However, 1D radial profiles are not sufficient to evaluate divertor power deposition in the presence of toroidal asymmetries. Recently, a 3D heat conduction solver code, TACO,[5] which uses a 3D time-resolved Fourier transform method, has been successfully implemented in the NSTX tokamak to acquire a 2D divertor heat flux distribution from the divertor surface temperature measured by infrared cameras. In addition, the code has been improved by incorporating a heat transmission coefficient, α, for the loosely held plasma-facing layer to reduce the negative heat flux, which is often calculated as a result of assuming that the surface is part of the substrate.[4] Additionally, the code utilizes a criterion of constant energy deposition after the end of discharge in order to choose an optimal value for α. In order to validate the results of calculated 2D divertor heat flux distribution, we compared the TACO results with those of THEODOR.

II. NSTX IR DIAGNOSTIC AND 2D HEAT FLUX DISTRIBUTION

NSTX has an open divertor (see Figure 1), and the primary first wall material is fine grain (ATJ) graphite. Magnetic field line radially expands at the divertor surface compared to the mid-plane and the multiplication factor, the so-called flux expansion, ranges from 5 to 30 and is typically higher than 10 for high elongation (κ, the shape parameter indicating how much the poloidal cross-section is stretched vertically) and

a)Author to whom correspondence should be addressed. Electronic mail: jahn@pppl.gov. Also at Princeton Plasma Physics Laboratory, Princeton, New Jersey 08543, USA.

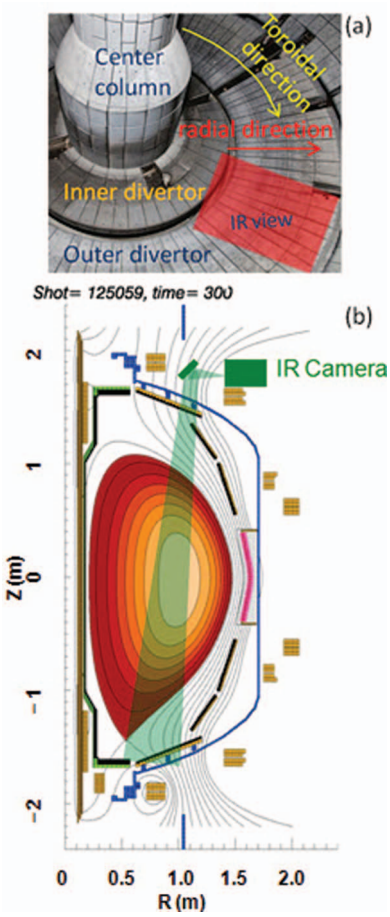

FIG. 1. (a) A photograph of NSTX lower divertor with the IR camera field of view indicated as a red shadowed region and (b) Plasma equilibrium and layout of the IR diagnostic.

triangularity (δ, the shape parameter for how close the cross-section is to the triangular shape) discharges. A high speed Santa Barbara Focal Plane IR camera (SBF161) was used to monitor the lower divertor thermal emission,[6] from which the surface heat flux was computed with a heat conduction model. The field of view of the IR camera can be changed to view the desired portion of the lower divertor with an adjustable mirror, as shown in Fig. 1. The detector of the IR camera was operated in the long wavelength IR (8–10μm) bandwidth with 128 × 128 pixels for the full frame, which gives a 5.8 mm spatial resolution on the divertor floor. The frame rate can be changed with different window size, from 1.6 kHz for the full frame and 6.3 kHz for 96 × 32 pixels. The IR camera views the divertor from the top of the machine, and can acquire a partial 2D divertor surface temperature distribution as shown in Fig. 1.

The original version of TACO inverts the measured 2D surface temperature to the heat flux distribution;[5] this version was developed at the COMPASS-D tokamak and was recently reused in MAST.[7] The tile front surface facing the plasma is defined as $z = 0$ and the rear surface is set to be at $z = \delta$, where δ is the tile thickness. For the NSTX outer target tiles, the thickness is 2.8 cm, while it is 5.1 cm for the inner tiles. Heat flux profiles presented in this paper are all for the outer strike point at the outer divertor tiles, as shown in Figure 1. Room temperature ($T = T_o$) is defined as the rear surface condition.

In numerical tests using the finite difference method to estimate the temperature rise by a constant heat load on the front tile face of up to 5 MW/m^2, it is found that the rear tile surface temperature shows almost no change after 1 s. It is therefore a good approximation to set $\delta = 2.8$ cm since a typical NSTX discharge only lasts ~1 s. This also justifies not considering materials on which the ATJ graphite tiles are fastened in the heat conduction equation. The thermal parameters used in the present version of TACO for the work in this paper are temperature dependent, compared to the constant thermal parameters used in the original version. Also, NSTX divertor target tiles are inertially cooled.

The partial differential equation to be solved is then the heat conduction equation in Cartesian coordinates:

$$\frac{\partial T}{\partial t} = \chi \left(\frac{\partial^2 T}{\partial x^2} + \frac{\partial^2 T}{\partial y^2} + \frac{\partial^2 T}{\partial z^2} \right), \quad (1)$$

where T is the temperature and χ is the thermal diffusivity, m^2/s in the SI unit, $\chi = k/c\rho$ (k is the thermal conductivity in W/m K, c is the heat capacity, and ρ is the density of the tile material). TACO solves this equation using the Fourier transform in both the x and y directions and the Laplace transform in the time domain, along with the boundary conditions for the front and rear tile surfaces. The derivation of full solution to this equation is given in Ref. 5 and we present it in Appendix A with some minor corrections and refinements, given that this reference is not generally available to the public.

The calculated heat flux often results in large negative values, particularly after transient events such as ELMs or strike point sweeping. The negative heat flux is not physically reasonable since there is no source of cooling present at the divertor surface in NSTX. This is because the solution to Eq. (1) in the original version of TACO does not consider the presence of thin, poorly adhered hydrocarbon layers that form naturally on the divertor surface. This surface layer can produce higher emission than is expected from the bulk tile temperature and therefore leads to incorrect solution to the heat conduction equation. Figure 2 shows a 2D heat flux distribution just following an ELM peak as calculated by TACO from the measured surface temperature distribution in Fig. 2(a), without considering the effects of surface layers. Regions of negative heat flux can be seen in Fig. 2(b) in the private flux region of the divertor after the ELM peak. In order to address the effect of thin surface layer, the heat transmission coefficient of the layer is defined as $\alpha = k_{layer}/d$, i.e., as the surface layer thermal conductivity divided by the thickness of the layer,[4] and is introduced in the procedure of solving the heat conduction equation. The use of α then allows us to take account of the effect of surface emission of the thin layer even though k_{layer} and d cannot be precisely estimated. This technique was first implemented in THEODOR[4] and is now applied to TACO for the 3D heat flux calculation. The surface heat flux $Q_s = Q_{xy}$ includes an assumption of zero heat capacity of the surface layer.[8] Therefore, the incoming heat flux from the plasma, the heat flux in the surface layer, and the heat flux into the tile bulk material are equal. The relationship between the surface temperature, T, and the bulk

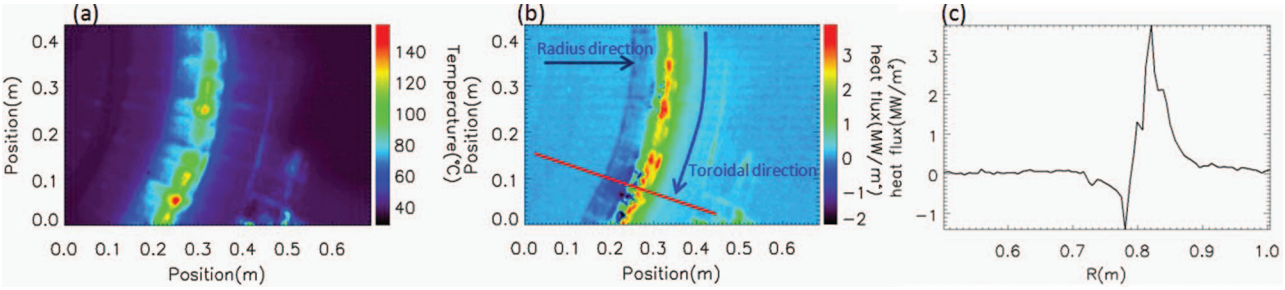

FIG. 2. (a) 2D temperature distribution after an ELM, (b) 2D divertor heat flux distribution calculated from (a) using the original version of TACO (no consideration of thin surface layer effect), and (c) 1D heat flux profile along the red radial line indicated in (b).

temperature of the ATJ graphite, T_{bulk}, therefore yields

$$Q = \alpha(T - T_{bulk}). \quad (2)$$

Note that T_{bulk} is the temperature used for the top surface of the tile in contact with the surface layer, so that, with the α parameter incorporated, we obtain a new solution to Eq. (1). The derivation of this solution is described in Appendix B. Another improvement we made compared to the original version of the code is that the thermal parameters are now temperature dependent to ensure a more accurate calculation.

We compare the results from TACO and THEODOR for the same toroidal angle in NSTX in order to benchmark the calculation. Figure 3 shows the comparison between TACO and THEODOR using $\alpha = 60\,000$ W m^{-2} K^{-1} for an ELMy discharge with $I_p = 800$ kA and $P_{NBI} = 4$ MW. It also had a similar magnetic configuration shown in Fig. 1(b). The radial line chosen to obtain 1D profile from the 2D TACO data is the same for the THEODOR calculation. The temporal evolution of peak heat flux values from TACO and THEODOR (Fig. 3(a)) is nearly identical during the inter-ELM period.

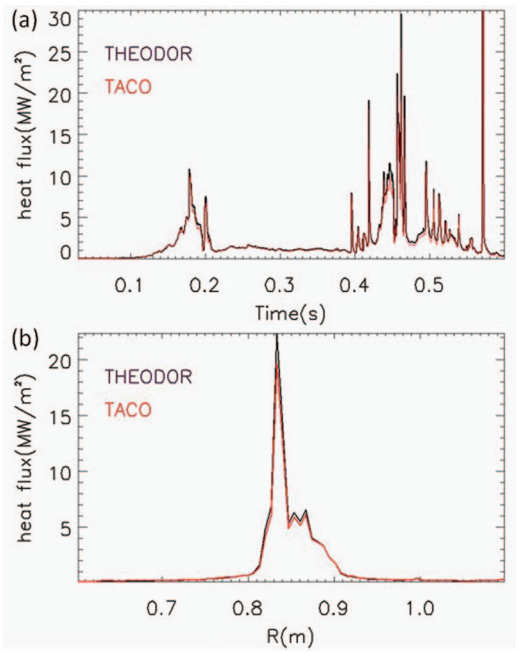

FIG. 3. Comparison of the result between TACO and THEODOR for the same radial line and 60 000 (W m^{-2} K^{-1}) α value; (a) Comparison of temporal evolution of peak heat flux and (b) Comparison of radial heat flux profiles at an ELM peak.

While the peak heat flux value from TACO is slightly higher than that of THEODOR during the ELMs. Heat flux radial profiles from TACO and THEODOR in Fig. 3(b) show very similar results between the two codes.

Note that TACO provides a 2D heat flux distribution, from which the 1D radial heat flux profile in Fig. 3 was extracted. Figure 4 shows such an example with the same set of surface temperature data as in Fig. 2 and using an α value of 60 000 (W m^{-2} K^{-1}). The negative heat flux in Fig. 2 has almost disappeared in the newly calculated result and the maximum heat flux during the ELM is reduced to ~3 MW/m^2, ~25% less than that in Fig. 2.

III. ANALYSIS

The use of an α value has a particularly significant impact on the transient (e.g., ELM) peak heat flux; therefore it will result in the largest measurement error if we arbitrarily choose the α value.[2] For instance, in the MAST tokamak, plotting the areal integrated energy received at the divertor during the full length of the discharge against several α values produces a series of curves which can be compared with the total deposited energy calculated by Langmuir probe data. An optimal value for α was found at the knee of the curve.[9] Because the negative heat flux is calculated after transient events without α, the calculated deposited power will be smaller after an ELM than before it. In Ref. 9 the authors consider the deposited power before and after ELM to be equal and choose the α value according this condition.[8] In this paper, a simple criterion was applied for the choice of α: the total energy deposited

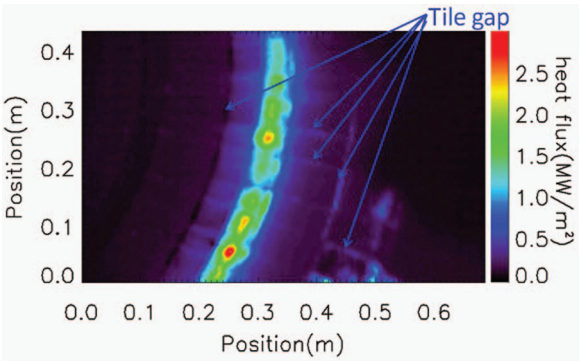

FIG. 4. The 2D heat flux distribution with 60 000 (W m^{-2} K^{-1}) α value. Some of the tile gaps are indicated with arrows.

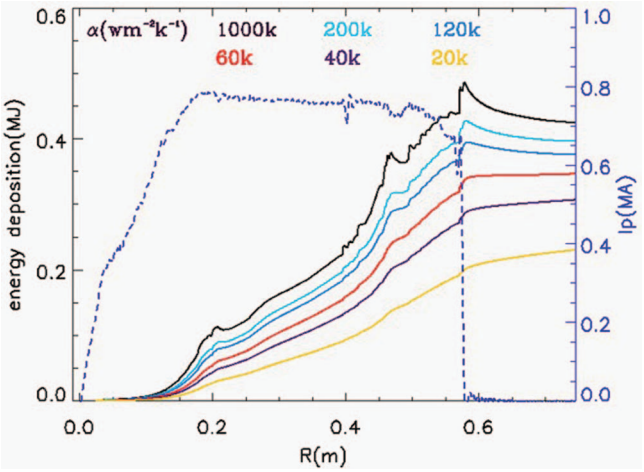

FIG. 5. Energy deposition calculated from the data by the IR camera, with different α values during and after the discharge.

in the divertor is obtained by integrating the power deposition in time, for which the power deposition was calculated from the 2D heat flux distribution from the TACO data. This takes full account of the measured 2D toroidal portion of the heat flux and would be more accurate than the simple toroidal integration of 1D heat flux profile from THEODOR. Temporal behavior of the estimated energy deposition after the end of discharge (i.e., when the heat deposited on the surface by the plasma is removed) is different for different α values with the end of discharge defined by the point of zero plasma current. Figure 5 shows the relationship between the energy deposition and the α value. It is found that the deposited energy decreases with time after the end of discharge with higher α values, e.g., 1 000 000 or 200 000 (W m^{-2} K^{-1}), which may have been caused by an overestimation of T_{bulk}. The higher the α value, the faster the deposited energy decreases. With a lower α value, e.g., 40 000 or 20 000 W m^{-2} K^{-1}, the energy deposition after the end of discharge increases because of the underestimated T_{bulk}. The lower the α value is, the faster the deposited energy increases. However, since there is no power going to the divertor after the end of discharge, the deposited energy should be constant after the discharge. As shown in Fig. 5, α = 60 000 (W m^{-2} K^{-1}) was chosen to keep the energy deposition constant after the end of discharge. This criterion can be also used in THEODOR or other finite difference heat conduction code using α to simulate the thin surface layer.

The obtained 2D heat flux distribution can be used in the study of various divertor heat flux physics. An example is the investigation of striated heat flux distribution in the 2D plane, caused by the ELM filaments, as shown in Fig. 6. 2D IR images have been used to study toroidally asymmetric heat deposition patterns during ELMs in other devices such as ASDEX-Upgrade,[10] but the actual 2D heat flux distribution has never been used for data analysis. In NSTX the magnetic flux expansion can be quite large; this is beneficial for the study of heat deposition from the ELM filaments because of the improved relative spatial resolution for each helical stripes compared to the low flux expansion case. Divertor heat flux studies traditionally focus on the 1D heat flux

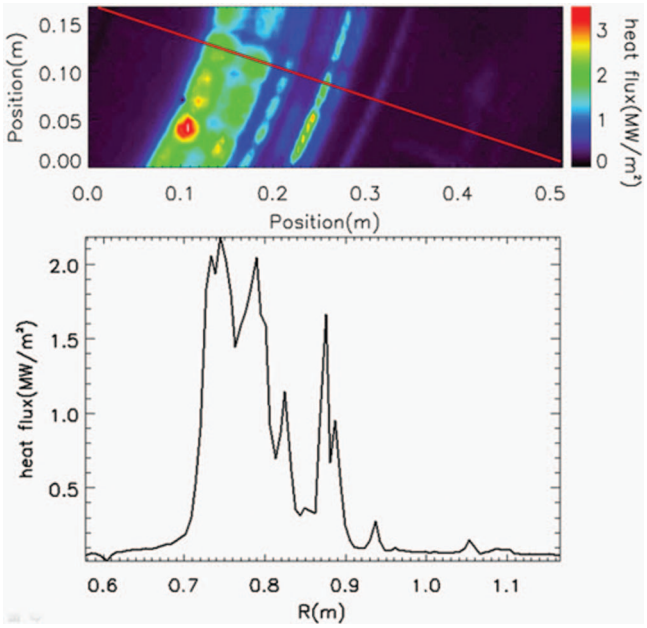

FIG. 6. Striated heat flux distribution at the divertor surface, (a) 2D heat flux distribution on the divertor surface with individual striations (from the ELM filaments) visible and (b) A 1D heat flux distribution along the red radial line indicated in (a).

distribution with a peak value at the strike point position. However, when ELM filaments exist they naturally carry hot and dense plasma particles to the divertor surface producing multiple local peaks in the heat flux profile at locations other than the strike point, as shown in Fig. 6. From Fig. 6(a), approximately 4–5 distinct toroidal striations can be identified within the given radial range. The 1D heat flux profile derived from Fig. 6(a) for the radial line indicated is given in Fig. 6(b). Fine structures in the heat flux at the divertor surface are reflected in the 2D profile such as the tile gaps and local peaks.

Another example of the use of 2D heat flux data is the quantitative analysis of the toroidal degree of asymmetry[11] (we denote it as ε_{DA}) of the peak heat flux, q_{peak}, and heat flux width, λ_q. We first obtain q_{peak}, i.e., at the strike point, of 1D heat flux profile at each toroidal angle, and then take an average over the values for all toroidal angles. This then represents the "mean peak heat flux" for the whole 2D plane observed by the IR camera ($\bar{q}_{peak}$). As for the definition of λ_q, $\lambda_q = P/(2\pi R_{peak} q_{peak})$, we use the integrated divertor power P (obtained directly from the 2D heat flux data, i.e., heat flux times area, with the fraction of area by the 2D IR camera coverage taken into account, all for the outer lower divertor for the data presented in this paper) and R_{peak} is the radial location of q_{peak} at each toroidal location. This yields a toroidal array of λ_q, from which a "mean heat flux width" can be also obtained ($\bar{\lambda}_g$) by taking an average over all λ_q values. The toroidal ε_{DA} of q_{peak} and λ_q represents the whole 2D plane observed by the IR camera as a function of time and is defined as $\varepsilon_{DA}(q_{peak}) = \sigma_{qpeak}/\bar{q}_{peak}$ and $\varepsilon_{DA}(\lambda_q) = \sigma_{\lambda q}/\bar{\lambda}_q$. Here, σ is the standard deviation of q_{peak} and λ_q over data in the toroidal array and this is normalized, respectively, by mean values of q_{peak} and λ_q to produce ε_{DA} at each time slice. In the case of ELMs, the helical heat deposition produces additional scatter

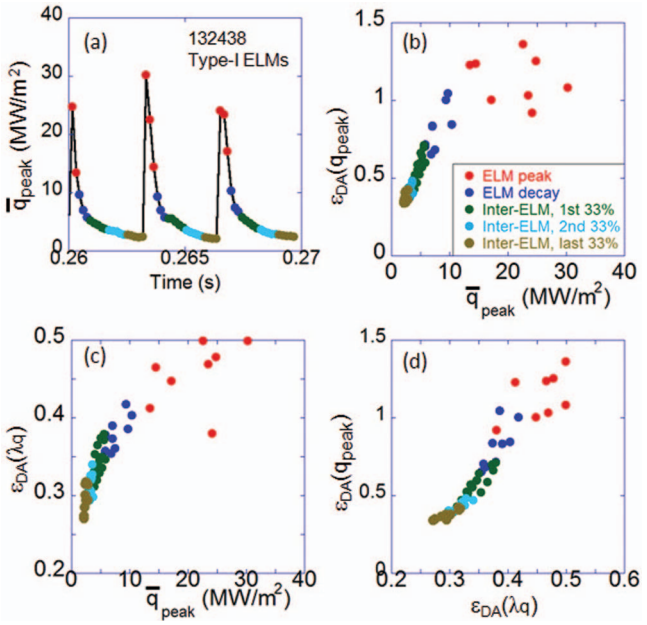

FIG. 7. (a) Temporal evolution of measured mean peak heat flux ($\bar{q}_{peak}$) during a type-I ELMy H-mode, (b) Toroidal degree of asymmetry for q_{peak}, ε_{DA} (q_{peak}), (c) Toroidal ε_{DA} (λ_q) as a function of $\bar{q}_{peak}$, and (d) Relation between ε_{DA} (λ_q) and ε_{DA} (q_{peak}). Data for each of the 1/3 of the ELM cycle have been colored green, sky blue, and gold, respectively.

of data around mean values to the background scatter level and it raises ε_{DA} for both q_{peak} and λ_q.

Figure 7 shows the result for a type-I ELMy H-mode, color-coded during the ELM cycle, across several ELMs. It is found that both ε_{DA} (q_{peak}) and ε_{DA} (λ_q) are largest at the ELM peak times and ε_{DA} (q_{peak}) can be as high as ~1.4 while ε_{DA} (λ_q) can reach up to ~0.5 for the dataset examined in Figure 7. Both ε_{DA} values increase with increasing q_{peak} and therefore the degree of asymmetric heat deposition is highest at the ELM peak times, while it becomes lower toward the later stage of the inter-ELM period (see Figures 7(b) and 7(c)). This dependence of the degree of asymmetric heat deposition on the ELM cycle is also related to the absolute value of peak heat flux. That is, higher peak heat flux leads to stronger degree of asymmetric q_{peak} and λ_q. It is also found from Fig. 7(d) that the correlation between ε_{DA} (q_{peak}) and ε_{DA} (λ_q) is the strongest at the ELM peak times and becomes weaker later in the ELM cycle.

IV. DISCUSSION

The fast IR data for the data analysis in this paper did not have coverage of inner strike point, so the choice of α parameter based on the energy balance described in Sec. III (see Figure 5) is only for the outer target. In fact, the characteristics of surface layer could vary spatially (e.g., from tile to tile and particularly between the inner and outer targets[8]), so that the use of a single α value would not perfectly fit for all divertor surfaces. The determined α value from the method employed in this paper represents the average over this possible spatial variation within the camera's field of view (FoV). Given that our data are all for the outer target, we presume the variation would be less than the case of the difference between inner and outer targets. Ideally, we would need a treatment with spatially varying α parameter but at present this average approach appears reasonable. We have not observed in the present data analysis a significant impact of spatially varying surface layers, e.g., local hot spots, on the asymmetry data presented in this study. For example, data for ε_{DA} (q_{peak}) as a function of q_{peak} for many ELM peak times with different location of strike points show a consistent single trend.

Comparison of energy deposition from the IR measurement with that from calorimetry data such as the tile embedded thermocouples[8] would have been very useful to cross-check the validity of the α selection method employed in this paper. However, NSTX thermocouple data were only taken with 1 min time resolution, which is not fast enough to obtain the decay length of tile temperature after the end of the discharge.

Another standard way of checking the energy balance of measured heat flux is to compare the ELM energy loss from the IR measurement ($\Delta W_{ELM,IR}$) to that from the diamagnetic plasma stored energy ($\Delta_{WELM,\,dia}$). The integral power obtained from the 2D heat flux profile is integrated in time to produce the deposited energy onto the divertor tiles. One problem for the dataset presented in this paper is that there is no IR measurement for the inner divertor, which significantly limits our ability to do the energy balance study. Nonetheless, Figure 8 shows the comparison of the outer divertor data with the fast diamagnetic data. Here, we used $\alpha = 40\,000$ (W m^{-2} K^{-1}) to get constant energy deposition after the discharge. It is seen that the majority of the data are distributed between $1/4\Delta W_{ELM,dia}$ and $1/2\Delta W_{ELM,dia}$. The ratio of ELM energy loss measured by the IR data (sum of inner and outer data) to that from the fast diamagnetic data is reported to be 0.4–0.7 in JET.[8] Also, the ELM energy loss on the inner divertor is reported similar to or slightly higher than that on the outer divertor.[8] If we assume that energy deposition is similarly split between the inner and outer, the measured IR ELM energy loss accounts for approximately 50%–100% of the ELM energy loss measured by the fast diamagnetic data. Of course there is no guarantee that the in/out energy split

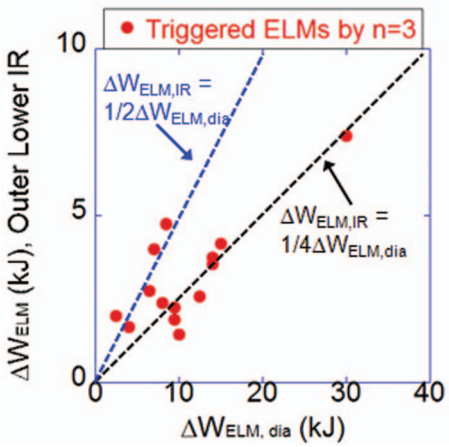

FIG. 8. Comparison of ELM energy deposition onto the outer divertor target, from the IR camera measurement to the ELM energy loss from the fast diamagnetic measurement. These data points use $\alpha = 40\,000$ W m^{-2} K^{-1}.

in NSTX should be the same as in JET, but the present IR dataset appears to account for approximately right fraction of the ELM energy loss, with the use of α parameter determined by the method described in the 1st paragraph of Sec. III.

V. SUMMARY AND CONCLUSIONS

A 3D heat conduction code, TACO, has been successfully implemented in NSTX to allow for the calculation of 2D heat flux distribution on the plasma-facing surface with a heat transmission coefficient, the so-called α parameter. A method for selecting the optimal α value was chosen to keep the energy deposition constant after the end of discharge and reduce the occurrence of negative heat fluxes, thus obtaining a more accurate heat flux result compared to the original version of TACO. In order to benchmark the calculated 2D divertor heat flux, the result from TACO was compared with one from a 2D heat conduction code THEODOR for the radial heat flux data at the same toroidal angle. It was shown that the peak heat fluxes were almost the same as the THEODOR values during inter-ELM periods, and slightly higher during the ELMs. Compared to the conventional 1D heat flux data, the 2D data provide an excellent means to investigate non-axisymmetric divertor heat flux physics such as striated heat flux patterns and the toroidal degree of asymmetry of q_{peak} and λ_q at the divertor surface, for example, caused by ELMs.

ACKNOWLEDGMENTS

This work was supported by the U.S. Department of Energy, Contract Nos. DE-AC05-00OR22725 and DE-AC02-09CH11466. K. F. Gan was supported by the National Magnetic Confinement Fusion Science Program of China under Contract No. 2011GB107001. One of the authors (J.-W. Park) was supported by the National Research Foundation of Korea with a grant funded by the Korean government, Contract No. 2012-0000590. The authors are grateful to Dr. A. Kirk and Dr. E. Delchambre for letting the NSTX team implement the original version of TACO for the implementation at PPPL.

APPENDIX A: DERIVATION OF HEAT FLUX SOLUTION IN TACO

The heat conduction equation to be solved is a partial deferential equation (PDE) in Cartesian coordinate for the divertor tile:

$$\frac{\partial T}{\partial t} = \chi \left(\frac{\partial^2 T}{\partial x^2} + \frac{\partial^2 T}{\partial y^2} + \frac{\partial^2 T}{\partial z^2} \right), \tag{A1}$$

where T is the temperature and χ is the thermal diffusivity, m^2/s in the SI unit.

Using the Fourier transform in both the x and y directions yields,

$$\frac{\partial T_{xy}}{\partial z} = \chi \left(\frac{\partial^2 T_{xy}}{\partial z^2} - \left(k_x^2 + k_y^2\right) T_{xy} \right), \tag{A2}$$

where the subscript xy indicates the transformed temperature and k_x and k_y are the transform variables. The remaining PDE can be reduced to a simple ordinary differential equation (ODE) by performing a Laplace transform with respect to t. With p as the Laplace transform variable, we obtain

$$\frac{\partial^2 \overline{T_{xy}}}{\partial z^2} - \left(p/\chi + k_{xy}^2\right)\overline{T_{xy}} = 0, \tag{A3}$$

where $k_{xy}^2 = k_x^2 + k_y^2$.

This has a solution in exponentials:

$$\overline{T_{xy}} = A \exp\left(\sqrt{\left(p/\chi + k_{xy}^2\right)} z\right) + B \exp\left(-\sqrt{\left(p/\chi + k_{xy}^2\right)} z\right). \tag{A4}$$

In order to obtain constants A and B, we consider boundary conditions for the front ($z = 0$) and rear ($z = \delta$) face of the tile,

$$\overline{T}_{xy}(z = \delta) = 0 \quad \text{for rear surface,}$$

$$\overline{Q}_{xy} = -k \frac{\partial \overline{T}_{xy}}{\partial z} |_{z=0} \quad \text{for front surface,}$$

where $\overline{Q}_{xy}$ is the Laplace and Fourier transformed heat flux Q and k is the thermal conductivity (W/m K).

Using this boundary condition, Eq. (A4) becomes

$$\overline{T_{xy}} = \frac{\overline{Q_{xy}}}{k\sqrt{\left(p/\chi + k_{xy}^2\right)}} \frac{\exp\left(\sqrt{\left(p/\chi + k_{xy}^2\right)}(\delta - z)\right) - \exp\left(-\sqrt{\left(p/\chi + k_{xy}^2\right)}(\delta - z)\right)}{\exp\left(\sqrt{\left(p/\chi + k_{xy}^2\right)}\delta\right) + \exp\left(-\sqrt{\left(p/\chi + k_{xy}^2\right)}\delta\right)}. \tag{A5}$$

In order to obtain the surface heat flux, we set z = 0 in Eq. (A5),

$$\overline{T_{xy}} = \overline{Q_{xy}} \frac{\tanh\left(\sqrt{\left(p/\chi + k_{xy}^2\right)}\delta\right)}{k\sqrt{\left(p/\chi + k_{xy}^2\right)}}. \tag{A6}$$

The convolution theorem for Laplace transforms yields the relation

$$T_{xy} = \int_0^t Q_{xy}(t - \tau) L^{-1} \left(\frac{\tanh\left(\sqrt{\left(p/\chi + k_{xy}^2\right)}\delta\right)}{k\sqrt{\left(p/\chi + k_{xy}^2\right)}} \right) d\tau. \tag{A7}$$

Now we use the infinite series,

$$\frac{\tanh(w)}{w} = 2\sum_{m=1}^{\infty} \frac{1}{\frac{\pi^2}{4}(2m-1)^2 + w^2}. \tag{A8}$$

So,

$$L^{-1}\left(\frac{\tanh\left(\sqrt{(p/\chi + k_{xy}^2)}\delta\right)}{k\sqrt{(p/\chi + k_{xy}^2)}}\right) = \frac{2\chi}{\delta} L^{-1}\left(\sum_{m=1}^{\infty} \frac{1}{\frac{\chi\pi^2}{4\delta^2}(2m-1)^2 + \chi k_{xy}^2 + p}\right). \tag{A9}$$

Inverse Laplace transform can be easily performed to obtain

$$L^{-1}\left(\frac{\tanh\left(\sqrt{(p/\chi + k_{xy}^2)}\delta\right)}{k\sqrt{(p/\chi + k_{xy}^2)}}\right) = \frac{2\chi}{\delta}\sum_{m=1}^{\infty} \exp\left(-\left(\frac{\chi\pi^2}{4\delta^2}(2m-1)^2 + \chi k_{xy}^2\right)\tau\right). \tag{A10}$$

And we get,

$$T_{xy} = \frac{2\chi}{\delta k}\int_0^t Q_{xy}(t-\tau)\sum_{m=1}^{\infty} \exp\left(-\left(\frac{\chi\pi^2}{4\delta^2}(2m-1)^2 + \chi k_{xy}^2\right)\tau\right) d\tau. \tag{A11}$$

Let us assume that the heat flux spatial distribution is constant during each time step; $\Delta\tau$ is the time step between IR frames. $Q_{xy}((j-l)\Delta\tau)$ represents heat flux from t_{j-l-1} to t_{j-l}, where $t_{j-l} = (j-l)\Delta\tau$. Then Eq. (A11) can be rewritten as

$$\begin{aligned} T_{xy} &= \frac{2\chi}{\delta k}\sum_{l=0}^{j-1} Q_{xy}(t_{j-l})\int_{t_l}^{t_{l+1}}\left(\sum_{m=1}^{\infty}\exp\left(-\left(\frac{\chi\pi^2}{4\delta^2}(2m-1)^2 + \chi k_{xy}^2\right)\tau\right)\right)d\tau \\ &= \frac{2\chi}{\delta k}\sum_{l=0}^{j-1} Q_{xy}(t_{j-l})\sum_{m=1}^{\infty}\frac{\exp\left(-\left(\frac{\chi\pi^2}{4\delta^2}(2m-1)^2 + \chi k_{xy}^2\right)t_l\right) - \exp\left(-\left(\frac{\chi\pi^2}{4\delta^2}(2m-1)^2 + \chi k_{xy}^2\right)t_{l+1}\right)}{\frac{\chi\pi^2}{4\delta^2}(2m-1)^2 + \chi k_{xy}^2} \\ &= \frac{2\chi}{\delta k}\sum_{l=0}^{j-1} Q_{xy}(t_{j-l})\sum_{m=1}^{\infty}\frac{\exp\left(-\left(\frac{\chi\pi^2}{4\delta^2}(2m-1)^2 + \chi k_{xy}^2\right)l\Delta\tau\right)\left(1-\exp\left(-\left(\frac{\chi\pi^2}{4\delta^2}(2m-1)^2 + \chi k_{xy}^2\right)\Delta\tau\right)\right)}{\frac{\chi\pi^2}{4\delta^2}(2m-1)^2 + \chi k_{xy}^2}. \end{aligned} \tag{A12}$$

Defining $\beta_m = (\frac{\chi\pi^2}{4\delta^2}(2m-1)^2 + \chi k_{xy}^2)\Delta\tau$ gives

$$T_{xy}(t_j) = \frac{2\chi\Delta\tau}{\delta k}\sum_{l=0}^{j-1} Q(t_{j-l})\sum_{m=1}^{\infty}\frac{\exp(-l\beta_m)(1-\exp(-\beta_m))}{\beta_m}. \tag{A13}$$

We define C_l here,

$$C_l = \sum_{m=1}^{\infty}\frac{\exp(-l\beta_m)(1-\exp(-\beta_m))}{\beta_m}. \tag{A14}$$

Then Eq. (A13) can be rewritten

$$T_{xy}(t_j) = \frac{2\chi\Delta\tau}{\delta k}\sum_{l=0}^{j-1} Q(t_{j-l})C_l. \tag{A15}$$

We rewrite this equation as follows:

$$Q_{xy}(t_j) = \frac{k\delta}{2\chi\Delta\tau}\frac{T_{xy}(t_j)}{C_o} - \sum_{l=0}^{j-1} Q_{xy}(t_{j-\ell})\frac{C_l}{C_0}.$$

Considering the non-zero initial temperature, we get the final form of $Q_{xy}(t_j)$,

$$Q_{xy}(t_j) = \frac{k\delta}{2\chi\Delta\tau}\frac{(T_{xy}(t_j) - T_{xy}(t_0))}{C_o} - \sum_{l=1}^{j-1} Q_{xy}(t_{j-\ell})\frac{C_l}{C_0}. \tag{A16}$$

The solution for $Q(t)$ is then obtained by performing the inverse Fourier transform.

APPENDIX B: DERIVATION OF HEAT FLUX SOLUTION WITH SURFACE HEAT TRANSMISSION COEFFICIENT, α

In the presence of thin surface layer on top of the tile, its poor thermal contact with the tile causes artificially high IR emission, particularly when there is transient heat flux such as by ELMs. This high emission can be interpreted as a high surface temperature and misleads the heat flux computation. One way to deal with this situation is to assume that there is an excess temperature at the surface proportional to the incident heat flux:[4]

$$T - T_{bulk} = Q/\alpha, \tag{B1}$$

where T is the surface temperature, T_{bulk} is the temperature at the top surface of the tile in contact with the surface layer, α is the heat transmission coefficient (in W/m^2 K). If there is no surface layer, $\alpha \rightarrow \infty$ and $T_{bulk} \rightarrow T$. From Eq. (B2), the Fourier transformed bulk temperature can be written as $T_{xy,\,bulk} = T_{xy} - Q_{xy}/\alpha$. Taking this into Eq. (A16) yields,

$$Q_{xy}(t_j) = \left(\frac{T_{xy}(t_j) - T_{xy}(t_0)}{C_o} - \sum_{\ell=1}^{j-1} Q_{xy}(t_{j-\ell}) \frac{C_\ell}{C_0} \right) \Bigg/ \left(1 + \frac{k\delta}{2\chi \Delta\tau C_0 \alpha} \right). \quad \text{(B2)}$$

The solution for $Q(t)$ is then obtained again by inverse Fourier transforming $Q_{xy}(t)$.

[1]A. Herrmann, W. Junker, K. Gunther, S. Bosch, M. Kaufmann, J. Neuhauser, G. Pautasso, Th. Richter, R. Schneide, and ASDEX Upgrade Team, Plasma Phys. Controlled Fusion **37**, 17 (1995).

[2]W. Fundamenski, T. Eich, S. Devaux, S. Jachmich, M. Jakubowski, H. Thomsen, G. Arnoux, F. Militello, E. Havlickova, D. Moulton, S. Brezinsek, G. Maddison, K. McCormick, A. Huber, and JET-EFDA Contributors, Nucl. Fusion **51**, 083028 (2011).

[3]R. P. Wenninger, T. Eich, G. T. A. Huysmans, P. T. Lang, S. Devaux, S. Jachmich, F. Kochl, and JET-EFDA Contributors, Plasma Phys. Controlled Fusion **53**, 105002 (2011).

[4]A. Herrmann, in *Proceedings of the 28th EPS Conference on Controlled Fusion and Plasma Physics, Madeira, 2001*.

[5]G. Castle, "Theory and operating instructions for the taco_run code," COMPASS Note 97.16, UKAEA Fusion, 1997.

[6]J.-W. Ahn, R. Maingi, D. Mastrovito, and A. L. Roquemore, Rev. Sci. Instrum. **81**, 023501 (2010).

[7]E. Delchambre, G. Counsell, and A. Kirk, Plasma Phys. Controlled Fusion **51**, 055012 (2009).

[8]T. Eich, P. Andrew, A. Herrmann, W. Fundamenski, A. Loarte, R. A. Pitts, and JET-EFDA Contributors, Plasma Phys. Controlled Fusion **49**, 573–604 (2007).

[9]F. Lott, A. Kirk, G. F. Counsell, J. Dowling, D. Taylor, T. Eich, and A. Herrmann, J. Nucl. Mater. **337–339**, 786–790 (2005).

[10]T. Eich, A. Herrmann, J. Neuhauser, and ASDEX Upgrade Team, Phys. Rev. Lett. **91**, 195003 (2003).

[11]J.-W. Ahn, K. F. Gan, F. Scotti, J. D. Lore, R. Maingi, J. M. Canik, T. K. Gray, A. G. McLean, A. L. Roquemore, and V. A. Soukhanovskii, "Study of non-axisymmetric divertor footprints using 2-D IR and visible cameras and a 3-D heat conduction solver in NSTX," J. Nucl. Mater. (in press).